

- (76) R. G. Gillard and P. R. Mitchell, *Struct. Bonding (Berlin)*, **7**, 47 (1970).  
 (77) R. D. Gillard, "Physical Methods in Advanced Inorganic Chemistry", H. A. O. Hill and P. Day, Ed., Interscience, 1968.  
 (78) C. J. Hawkins, "Absolute Configuration of Metal Complexes", Wiley-Interscience, New York, N.Y., 1971.  
 (79) M. Ito, F. Marumo, and Y. Saito, *Acta Crystallogr., Sect. B*, **27**, 2187 (1971).  
 (80) A. G. McCaffery, S. F. Mason, and R. E. Bollard, *J. Chem. Soc.*, 5094 (1965).  
 (81) R. B. Von Dreele and R. C. Fay, *J. Am. Chem. Soc.*, **93**, 4936 (1971).  
 (82) M. R. Snow, *Acta Crystallogr., Sect. B*, **30**, 1850 (1974).  
 (83) K. R. Butler and M. R. Snow, *Chem. Commun.*, 550 (1971).

Contribution from the Department of Chemistry, Colorado State University, Fort Collins, Colorado 80523, and the Instituto de Química, Universidade de São Paulo, São Paulo, Brazil

## Ligand Oxidation in Iron Diimine Complexes. 3. Electrochemical Oxidation of Tris(glyoxal bis(methylimine))iron(II)

HELENA LI CHUM,\*<sup>1a</sup> T. RABOCKAI,<sup>1a</sup> J. PHILLIPS,<sup>1b</sup> and R. A. OSTERYOUNG\*<sup>1b</sup>

Received August 13, 1976

AIC60591B

The electrochemical oxidation of tris(glyoxal bis(methylimine))iron(II),  $\text{Fe}(\text{GMI})_3^{2+}$ , has been investigated using cyclic voltammetry and rotating-disk studies in 0.5 M  $\text{H}_2\text{SO}_4$ . The main reaction product is an iron(III) complex in which one of the GMI ligands is oxidized to  $\text{H}_3\text{CN}=\text{C}(\text{OH})\text{CH}=\text{NCH}_3$ , thus consuming  $3F/\text{mol}$  of  $\text{Fe}(\text{GMI})_3^{2+}$ . A reaction mechanism consisting of electrochemical oxidation of the Fe(II) to an Fe(III) complex followed by a rate-determining first-order chemical reaction is proposed. In this chemical reaction, the Fe(III) complex is intramolecularly reduced to the Fe(II) state, with concomitant oxidation of the ligand; the radical-ligand complex is then further electrochemically oxidized very rapidly. This proposed ECE mechanism is compatible with the experimental results. The rate for the intramolecular reduction of the ferric complex is  $22 \pm 2 \text{ s}^{-1}$ . This value is applied to estimate a second-order rate constant of  $10^9\text{--}10^{10} \text{ M}^{-1} \text{ s}^{-1}$  for the chemical oxidation of  $\text{Fe}(\text{GMI})_3^{2+}$  in this acid concentration.

### Introduction

In the first two papers of this series,<sup>2,3</sup> it has been shown that the chemical oxidation of the low-spin iron(II) complex of the diimine ligand glyoxal bis(methylimine) ( $\text{H}_3\text{CN}=\text{C}-\text{HCH}=\text{NCH}_3$ ),  $\text{Fe}(\text{GMI})_3^{2+}$ , by Ce(IV) proceeds via  $\text{Fe}(\text{GMI})_3^{3+}$ . This ferric complex undergoes an intramolecular one-electron transfer followed by the oxidation of this product by another  $\text{Fe}(\text{GMI})_3^{3+}$ , yielding two new ligand-oxidized complexes and regenerating  $\text{Fe}(\text{GMI})_3^{2+}$ . The rate of this disproportionation reaction depends very strongly on the acid concentration.<sup>3</sup> Spectrophotometric and potentiodynamic studies at 25 °C yielded for the disproportionation reaction the following second-order rate constants:  $(2.2 \pm 0.2) \times 10^3$  and  $(0.7 \pm 0.1) \times 10^3 \text{ M}^{-1} \text{ s}^{-1}$  in 4.0 and 5.0 M  $\text{H}_2\text{SO}_4$ , respectively. Using these techniques, it was not possible to obtain rate constants for  $\text{H}_2\text{SO}_4$  concentrations lower than 4.0 M. In 0.5 M  $\text{H}_2\text{SO}_4$  the reaction is faster than the upper limit of detection of stopped-flow techniques.<sup>3</sup> In 11 M  $\text{H}_2\text{SO}_4$ ,<sup>4</sup> a one-electron reversible oxidation of  $\text{Fe}(\text{GMI})_3^{2+}$  was observed.

The electrochemical oxidation of  $\text{Fe}(\text{GMI})_3^{2+}$  at low acid concentration (0.5 M  $\text{H}_2\text{SO}_4$ ) has now been studied by means of cyclic voltammetric and rotating-disk techniques and by coulometric oxidation. The coupling of these techniques enables us to propose a mechanism for the electrochemical oxidation of  $\text{Fe}(\text{GMI})_3^{2+}$ , to determine the rate constant for the intramolecular reduction of the ferric complex, and also to estimate the rate constant for the chemical oxidation at low acid concentration.

### Experimental Section

The chemicals used in this study are described in part 1.<sup>2</sup>

A Princeton Applied Research Corp. (PARC) Model 170 electrochemistry system coupled to a 564 Tektronix storage oscilloscope was used throughout the present work. Rotating-disk measurements employed the ASR2 analytical rotator from Pine Instruments Co.; the available rotation speed was 50–10 000 rpm. Coulometric experiments were performed with the PARC Model 173 potentiostat/galvanostat with a Model 176 digital coulometer.

The electrochemical cells were glass cylinders (75-mm i.d.  $\times$  75-mm height), closed with a tightly fitting Teflon cover which held the three electrodes and the gas inlet and outlet tubes. The working electrodes were glassy carbon disks (G.C. 30 rod 3-mm diameter from Tokai Electrode Manufacturing Co., Ltd., or from Pine Instruments, diameter

7 mm); a platinum wire and a saturated calomel electrode served as the auxiliary and reference electrodes.

A coulometric cell was made of a glassy carbon crucible (50-mm i.d.  $\times$  50-mm height) closed with a tightly fitting Teflon cover which held the reference and auxiliary electrodes and the inlet–outlet tubes. The solution was magnetically stirred so that the total electrolysis was achieved in less than 1 h.

Oxygen was removed by bubbling  $\text{N}_2$  through the solution for 30 min prior to the electrochemical measurements.

Visible absorption spectra were obtained with a Cary 17 spectrophotometer.

### Results and Discussion

Typical cyclic voltammograms of  $\text{Fe}(\text{GMI})_3^{2+}$  in 0.5 M  $\text{H}_2\text{SO}_4$ , for several scan rates, are shown in Figure 1. At slower scan rates, e.g.  $0.5 \text{ V s}^{-1}$  (Figure 1a), the first anodic sweep shows only one anodic current peak at 1.15 V vs. SCE. On the cathodic sweep, the corresponding cathodic peak was not observed but a new cathodic peak at 0.6 V vs. SCE was found. On the second cycle, the corresponding anodic current peak of the more easily oxidizable couple was seen, and a significant decrease of the anodic current peak for the starting material was observed. As the scan rate was increased (Figure 1b–d) it was possible to detect the cathodic current peak corresponding to the reduction of  $\text{Fe}(\text{GMI})_3^{3+}$ —i.e., the reduction of the product formed at 1.15 V vs. SCE.

Figure 2 shows the ratio of the anodic peak current ( $i_{pa}$ ) to the square root of scan rate ( $\nu^{1/2}$ ) plotted as a function of  $\nu^{1/2}$ . The ratio  $i_{pa}/\nu^{1/2}$  is independent of  $\nu^{1/2}$  for a diffusion-controlled process. Figure 2 shows that, for scan rates higher than  $50 \text{ V s}^{-1}$ , this behavior is achieved. At scan rates less than this, a chemical reaction generating another electroactive couple ( $E_{1/2} = 0.65 \text{ V vs. SCE}$ ) takes place.

Since no IR correction was applied to these measurements, the anodic to cathodic peak potential separation increased with scan rate and was larger than 59 mV, the value to be expected for a one-electron reversible process.<sup>5</sup> However, since the anodic to cathodic peak current ratio approached unity at  $100 \text{ V s}^{-1}$  and the anodic peak potential from 5 to  $50 \text{ V s}^{-1}$  was constant within the experimental error,  $1.15 \pm 0.01 \text{ V vs. SCE}$ , it is likely that the electrochemical oxidation of  $\text{Fe}(\text{GMI})_3^{2+}$  to  $\text{Fe}(\text{GMI})_3^{3+}$  is a reversible, diffusion-controlled process.

Using the plateau region of Figure 2, it is possible to calculate a diffusion coefficient for  $\text{Fe}(\text{GMI})_3^{2+}$  of  $(8.0 \pm 0.8)$

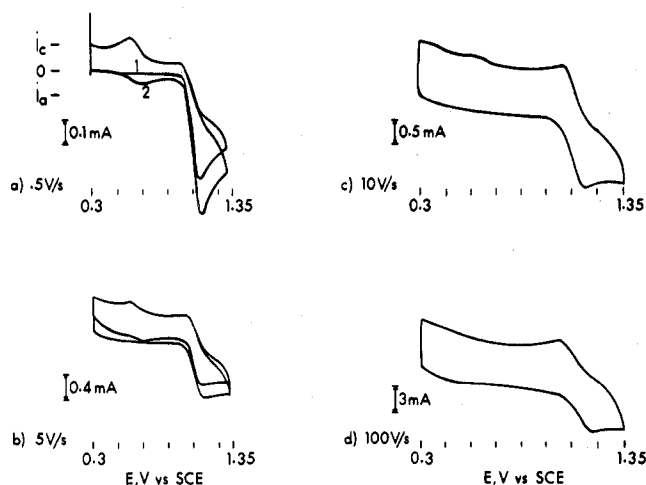


Figure 1. Cyclic voltammograms of a  $1.0 \times 10^{-3}$  M solution of  $\text{Fe}(\text{GMI})_3^{2+}$  in  $0.5 \text{ M H}_2\text{SO}_4$  on a glassy carbon working electrode at  $25^\circ\text{C}$ . Scan rates: (a) 0.5, (b) 5.0, (c) 10, and (d)  $100 \text{ V s}^{-1}$ .

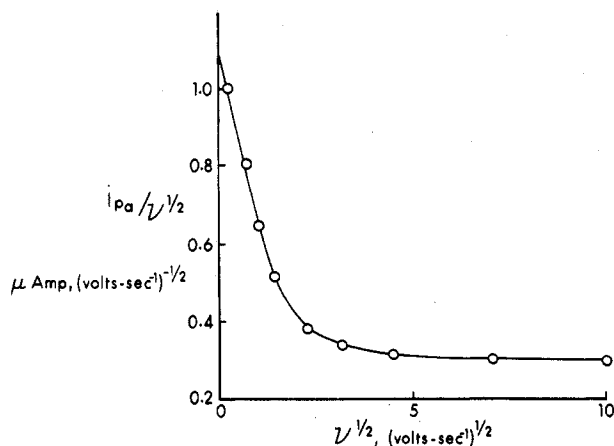


Figure 2. Dependence of  $i_{pa}/v^{1/2}$  as a function of  $v^{1/2}$  in the electrochemical oxidation of  $1.0 \times 10^{-3}$  M  $\text{Fe}(\text{GMI})_3^{2+}$  in  $0.5 \text{ M H}_2\text{SO}_4$  on a glassy carbon working electrode at  $25^\circ\text{C}$ .

$\times 10^{-6} \text{ cm}^2 \text{ s}^{-1}$ , using the Randles-Sevcik equation<sup>6</sup>

$$i_p = 2.67 \times 10^5 n^{3/2} A D^{1/2} C_0^b v^{1/2} \quad (25^\circ\text{C})$$

where  $D$  is the diffusion coefficient,  $A$  is the area of the working electrode,  $n$  is the number of electrons, and  $C_0^b$  is the bulk concentration of  $\text{Fe}(\text{GMI})_3^{2+}$ .

To determine the order of the following chemical reaction with respect to  $\text{Fe}(\text{GMI})_3^{3+}$ , a series of experiments as a function of the concentration of  $\text{Fe}(\text{GMI})_3^{2+}$  were performed using a rotating glassy carbon disk and varying the rotation speed from 50 to 10000 rpm. The concentration of the complex was varied by a factor of 125.

The Levich equation<sup>7</sup> expresses the limiting current as a function of the rotating speed

$$i_L = \frac{nFA C_0^b D^{2/3} \omega^{1/2}}{1.62 v^{1/6}} \quad (25^\circ\text{C})$$

where  $\omega$  is the angular velocity ( $\text{rad s}^{-1}$ ) and  $v$  is the kinematic viscosity ( $\text{cm}^2 \text{ s}^{-1}$ ). Simple diffusion-controlled processes yield linear plots of  $i_L$  as a function of  $\omega^{1/2}$ , passing through the origin.

A plot of  $i_L/(C_0^b \omega^{1/2})$  as a function of  $\omega^{1/2}$  for three different complex concentrations is shown in Figure 3. This plot is analogous to that of Figure 2. However, within the accessible experimental range of rotation speeds, the plateau of the curve in Figure 3 is not reached, as observed in Figure 2. Also shown

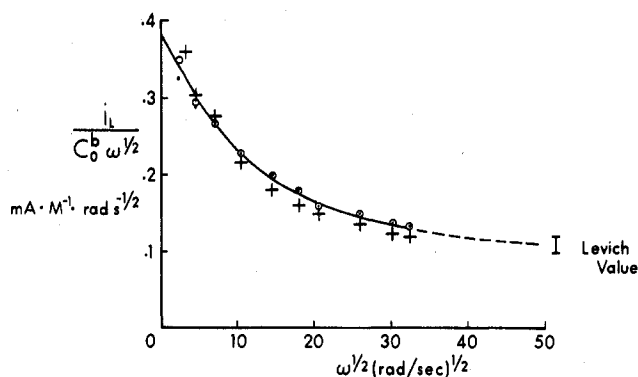


Figure 3. Dependence of  $i_L/C_0^b \omega^{1/2}$  as a function of rotation speed ( $\omega^{1/2}$ ) in the electrochemical oxidation of  $\text{Fe}(\text{GMI})_3^{2+}$  in  $0.5 \text{ M H}_2\text{SO}_4$  on a glassy carbon working electrode at  $25^\circ\text{C}$ . Complex concentrations: (●)  $1.0 \times 10^{-3}$  M; (○)  $0.5 \times 10^{-3}$  M; (+)  $0.1 \times 10^{-3}$  M.

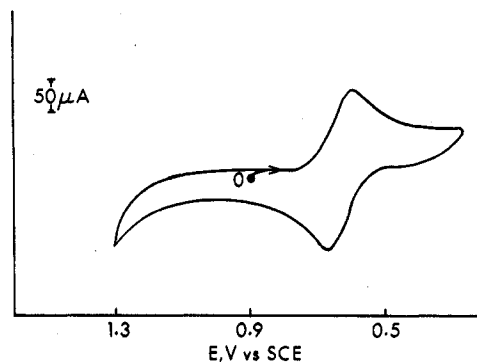


Figure 4. Cyclic voltammogram of a  $8.9 \times 10^{-4}$  M solution of  $\text{Fe}(\text{GMI})_2(\text{GA})^{3+}$ , obtained in the oxidation of a  $1.2 \times 10^{-3}$  M solution of  $\text{Fe}(\text{GMI})_3^{2+}$  by 4.5 equiv of  $\text{Ce}(\text{IV})$ , in  $0.5 \text{ M H}_2\text{SO}_4$ .

in Figure 3 is the value of  $i_L/(C_0^b \omega^{1/2})$  which would be achieved for the simple oxidation of  $\text{Fe}(\text{GMI})_3^{2+}$  to  $\text{Fe}(\text{GMI})_3^{3+}$ , calculated using the Levich equation and the diffusion coefficient obtained from cyclic voltammetric measurements. It is also evident from Figure 3 that  $i_L/(C_0^b \omega^{1/2})$  is independent of the concentration of complex, within the experimental error, thus indicating a first-order following chemical reaction.

Plots of the general type of Figure 3 are characteristic of chemical reactions (C) coupled between electrochemical (E) reactions. Many examples of  $\text{ECE}^{8-10}$  or  $\text{ECEC}^{11}$  mechanisms have been studied by rotating-disk experiments.

From Figure 2 or 3 it is possible to calculate the number of electrons associated with the overall reaction, as compared to the number of electrons associated with the simple one-electron oxidation of the ferrous to ferric complex<sup>12</sup>

$$\begin{aligned} \frac{n_{\text{overall}}}{n_{\text{Fe}(\text{GMI})_3^{2+}/\text{Fe}(\text{GMI})_3^{3+}}} &= \frac{(i_{pa}/v^{1/2})_{v^{1/2}=0}}{(i_{pa}/v^{1/2})_{v^{1/2}=\infty}} \\ &= \frac{(i_L/C_0^b \omega^{1/2})_{\omega^{1/2}=0}}{(i_L/C_0^b \omega^{1/2})_{\omega^{1/2}=\infty}} = 3.3 \pm 0.4 \end{aligned}$$

To establish the nature of the redox couple formed after the electrochemical step, consuming ca.  $3F/\text{mol}$  of  $\text{Fe}(\text{GMI})_3^{2+}$ , the cyclic voltammograms in Figure 1 were compared with those in Figures 4 and 5, which present cyclic voltammograms of the reversible oxidation of  $\text{Fe}(\text{GMI})_2(\text{GA})^{3+}$  ( $\text{GA} = \text{H}_3\text{C}=\text{C}(\text{OH})\text{CH}=\text{NCH}_3$ ) generated by chemical oxidation of  $\text{Fe}(\text{GMI})_3^{2+}$  by  $\text{Ce}(\text{IV})$  (4.5 equiv of  $\text{Ce}(\text{IV})/\text{mol}$  of  $\text{Fe}(\text{GMI})_3^{2+}$ ). Under these conditions 75–80% of  $\text{Fe}(\text{GMI})_3^{2+}$  is converted to  $\text{Fe}(\text{GMI})_2(\text{GA})^{3+}$ , consuming 3 equiv of  $\text{Ce}(\text{IV})/\text{mol}$  of  $\text{Fe}(\text{GMI})_3^{2+}$ . The remaining oxidation

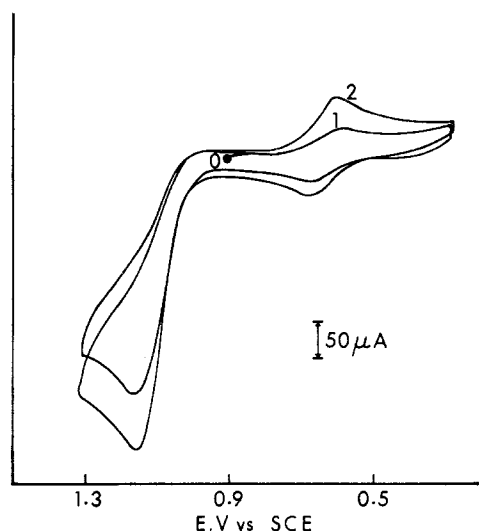


**Figure 5.** Cyclic voltammogram of a mixture of  $\text{Fe}(\text{GMI})_3^{2+}$  (66%),  $\text{Fe}(\text{GMI})_2(\text{GA})^{3+}$  (23%), and  $\text{Fe}(\text{GMI})_2(\text{GH})^{2+}$  (12%) obtained by oxidizing a  $1.2 \times 10^{-3}$  M solution of  $\text{Fe}(\text{GMI})_3^{2+}$  with 1 equiv of  $\text{Ce}(\text{IV})$ /mol of complex, in 0.5 M  $\text{H}_2\text{SO}_4$ ; scan rate  $0.2 \text{ V s}^{-1}$ ,  $25^\circ \text{C}$ .

equivalents are consumed to form 20–25% of several very labile complexes in which ligand oxidation proceeds further, with the consumption of 5–9 equiv of  $\text{Ce}(\text{IV})$ /mol of  $\text{Fe}(\text{GMI})_3^{2+}$  ( $-\text{CH}=\text{N}-(-2e) \rightarrow -\text{C}(\text{OH})=\text{N}-$  and  $=\text{NCH}_3(-2e) \rightarrow =\text{NCH}_2\text{OH}(-2e) \rightarrow =\text{NCHO}(-2e) \rightarrow =\text{NCOOH}$ ).<sup>3</sup> In the initial stages of the reaction, only  $\text{Fe}(\text{GMI})_2(\text{GA})^{3+}$  and  $\text{Fe}(\text{GMI})_2(\text{GH})^{2+}$  ( $\text{GH} = \text{H}_3\text{CN}=\text{CHCH}=\text{NCH}_2\text{OH}$ ) were found.<sup>3</sup> The modification introduced in the ligand GH is very distant from the diimine chromophore<sup>13,14</sup> which determines the properties of the compound. For this reason, this complex has the same  $E_{1/2}$  as the  $\text{Fe}(\text{GMI})_3^{3+}/\text{Fe}(\text{GMI})_3^{2+}$  couple, as can be seen on the cyclic voltammograms in Figure 5 for a mixture of  $\text{Fe}(\text{GMI})_3^{2+}$  (66%),  $\text{Fe}(\text{GMI})_2(\text{GA})^{3+}$  (25%), and  $\text{Fe}(\text{GMI})_2(\text{GH})^{2+}$  (12%) obtained by oxidation of  $\text{Fe}(\text{GMI})_3^{2+}$  with 1 equiv of  $\text{Ce}(\text{IV})$ . The cyclic voltammogram (Figure 5) displays only the oxidation peak at 1.15 V vs. SCE and the oxidation and reduction peaks at around 0.65 V vs. SCE, corresponding as shown in Figure 4, to the couple  $\text{Fe}(\text{GMI})_2(\text{GA})^{3+}/\text{Fe}(\text{GMI})_2(\text{GA})^{2+}$ . We conclude that the peaks at 1.15 V must correspond to the oxidation of two very similar ferrous complexes.

The cyclic voltammogram obtained after total electrolysis of  $\text{Fe}(\text{GMI})_3^{2+}$  ( $4.1F$ /mol of  $\text{Fe}(\text{GMI})_3^{2+}$ , 60 min) is shown in Figure 6. Only one anodic and one cathodic current peak, at the same potentials observed for the  $\text{Fe}(\text{GMI})_2(\text{GA})^{3+}/\text{Fe}(\text{GMI})_2(\text{GA})^{2+}$  couple are seen. After partial electrolysis ( $1.0F$ /mol of  $\text{Fe}(\text{GMI})_3^{2+}$ , 2 min), the cyclic voltammogram shown in Figure 7 was obtained. Comparison between Figures 5 and 7 clearly indicates that  $\text{Fe}(\text{GMI})_2(\text{GA})^{3+}$  was formed in both cases in approximately the same proportion ( $23 \pm 2\%$ ). These data correspond, however, to fast oxidations, either chemically (1 min) or electrochemically (2 min). These reaction times are comparable to the time range employed in the slow cyclic voltammetry and rotating-disk experiments. The longer the reaction times, e.g., total electrolysis, the greater the importance of the secondary reaction processes that complicate the system.

These data indicate that the product with  $E_{1/2} = 0.65 \text{ V}$  vs. SCE formed during the cyclic voltammograms (Figure 1) is  $\text{Fe}(\text{GMI})_2(\text{GA})^{3+}$ . To further corroborate this assignment, visible absorption spectra of the inert products of electrochemical and of chemical oxidation were compared. The chemical product exhibits a very broad asymmetric band,  $\lambda_{\text{max}}$  580 nm, half-width (+) =  $0.020 \mu\text{m}^{-1}$ . The inert product of coulometric oxidation displays the same characteristics, thus

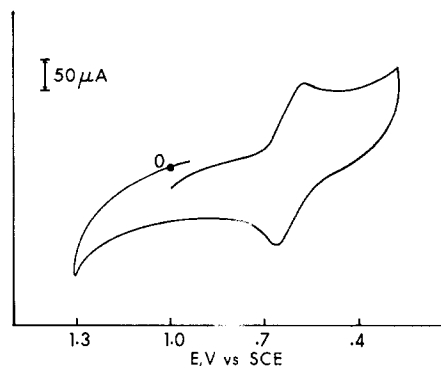


**Figure 6.** Cyclic voltammogram of the final inert oxidation product of  $\text{Fe}(\text{GMI})_3^{2+}$  after coulometric oxidation on a glassy carbon crucible at 1.3 V vs. SCE.

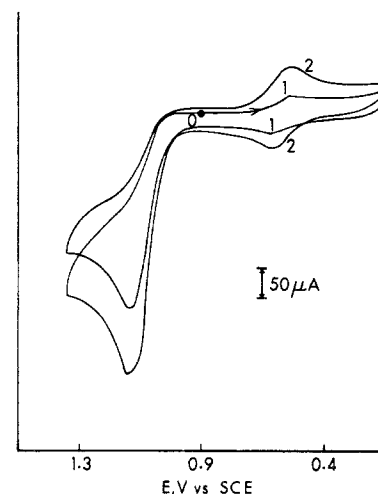
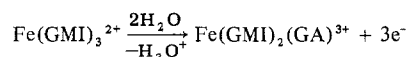


**Figure 7.** Cyclic voltammogram of a  $1.25 \times 10^{-3}$  M solution of  $\text{Fe}(\text{GMI})_3^{2+}$  after electrolysis ( $1F$ /mol of complex); scan rate  $0.2 \text{ V s}^{-1}$ ,  $25^\circ \text{C}$ ,  $[\text{H}_2\text{SO}_4] = 0.5 \text{ M}$ .

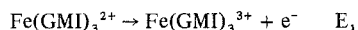
corroborating the identification of the major product of electrochemical oxidation.

The overall number of electrons obtained from the relatively fast rotating-disk and cyclic voltammetry experiments indicates that the major oxidation product (80–90%) consumes  $3F$ /mol of  $\text{Fe}(\text{GMI})_3^{2+}$ . Approximately 10–20% of secondary products consume  $\geq 5F$ /mol of  $\text{Fe}(\text{GMI})_3^{2+}$ .

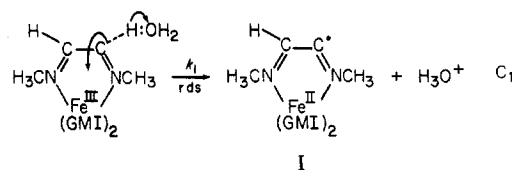
The major electrochemical oxidation of  $\text{Fe}(\text{GMI})_3^{2+}$  can thus be described as



As indicated by the cyclic voltammetric experiments at fast scan rate, the primary step of oxidation is the formation of  $\text{Fe}(\text{GMI})_3^{3+}$ , a diffusion-controlled process



As indicated by the shape of  $i_{\text{pa}}/\nu^{1/2}$  vs.  $\nu^{1/2}$  and  $i_L/(C_0^b\omega^{1/2})$  vs.  $\omega^{1/2}$  plots, chemical and electrochemical reactions follow this electrochemical step. In analogy to the mechanism proposed for the chemical oxidation,<sup>3</sup> the next step should be an intramolecular electron transfer,<sup>15</sup> assisted by nucleophilic attack of the solvent, water



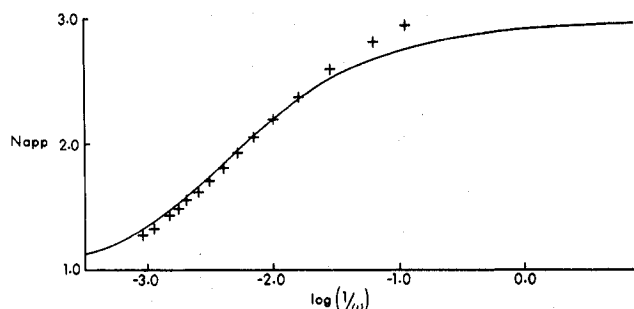
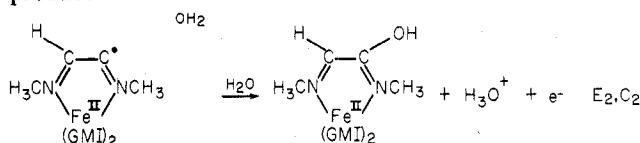
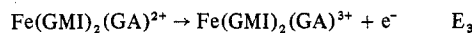


Figure 8. Plot of  $N_{app}$  vs.  $\log(1/\omega)$ . Solid line shows calculated curve using  $k = 22 \pm 2 \text{ s}^{-1}$ ,  $D = (8.0 \pm 0.8) \times 10^{-6} \text{ cm}^2 \text{ s}^{-1}$ , and  $\nu = 0.011$  p. Plus signs show the experimental data obtained from rotating-disk studies. Each experimental point is an average of six determinations on four different complex concentrations.

Since species I is not stabilized by resonance through the  $\pi$  diimine system, the radical complex (I) should be readily oxidized at potentials corresponding to the oxidation of  $\text{Fe}(\text{GMI})_3^{2+}$ . By addition of  $\text{H}_2\text{O}$  to the oxidation product—a step that is probably concerted with the electrochemical step<sup>15</sup>—the ligand-oxidized product in the  $\text{Fe}(\text{II})$  form is produced



Finally, since the potential of the primary step ( $\text{E}_1$ ) is approximately 0.4 V more positive than the  $\text{E}_{1/2}$  for the oxidation of the couple  $\text{Fe}(\text{GMI})_2(\text{GA})^{3+}/\text{Fe}(\text{GMI})_2(\text{GA})^{2+}$ , further oxidation occurs very rapidly—i.e.



Recently, Richter, Daul, and Zelewsky<sup>16</sup> were able to generate electrolytically a radical–ligand complex of the aliphatic diimine ligand glyoxal bis(butylimine) with zinc ions and to detect its EPR spectrum and reactivity. This species is analogous to the proposed radical complex I.

The mechanism proposed here for the electrochemical oxidation of  $\text{Fe}(\text{GMI})_3^{2+}$  is an ECE type. Since  $\text{C}_1$  is rate determining and  $\text{C}_2$  close to the diffusion limit, the second electrochemical step appears as the composite of  $\text{E}_2$  and  $\text{E}_3$ .

A modification<sup>17</sup> of Karp's procedure<sup>18</sup> to the study of homogeneous kinetics with the rotating disk, taking into account a two-electron second electrochemical step, yields a rate constant of  $22 \pm 2 \text{ s}^{-1}$  for the chemical rate-determining reaction. Figure 8 shows the working curve calculated for the present system and the experimental data. The agreement of experimental and calculated data is excellent except in regions of very fast or very slow rotation speeds. At slow rotation speeds, the participation of the secondary oxidation processes is more important, thus explaining the systematic positive deviation of the experimental points in these conditions. These results are in accord with the proposed reaction mechanism.<sup>19</sup>

The rate constant for the intramolecular reduction of the ferric complex provides an estimate for the rate constant of the chemical oxidation of  $\text{Fe}(\text{GMI})_3^{2+}$  at this low acid concentration. The kinetics of this reaction are second order in  $\text{Fe}(\text{GMI})_3^{3+}$ .<sup>3</sup> It is proposed that the radical complex (I) (steady-state concentration  $\sim 10^{-6}$ – $10^{-7} \text{ M}$ ,  $\epsilon_{\text{max}} \sim 10^3$ ) is formed by an intramolecular reduction analogous to  $\text{C}_1$ , with a rate constant  $k_1$ . A back-reaction of  $\text{C}_1$  ( $k_{-1}$ ) would explain

the sensitivity of the overall rate constant to proton and water activities. The next step is the oxidation of the radical complex (I) by another  $\text{Fe}(\text{GMI})_3^{3+}$  ion. Let us assume that this reaction has a rate constant ( $k_{\text{exc}}$ ) of  $10^7$ – $10^8 \text{ M}^{-1} \text{ s}^{-1}$ , based on the rate of exchange of electrons in systems of the diimine type, e.g.,  $\text{Fe}(\text{phen})_3^{3+}/\text{Fe}(\text{phen})_3^{2+}$ , which is  $3 \times 10^8 \text{ M}^{-1} \text{ s}^{-1}$ .<sup>20</sup> The overall rate equation for the chemical oxidation<sup>3</sup> is  $-\text{d}[\text{Fe}(\text{GMI})_3^{3+}]/\text{dt} \approx 3(k_1/k_{-1})_{\text{exc}}[\text{Fe}(\text{GMI})_3^{3+}]^2$ . The overall rate constant can be estimated, if one assumes  $k_{-1} \leq 1 \text{ s}^{-1}$ , as  $3 \times 2 \times 10 \times (10^7\text{--}10^8)$ , of the order of  $10^9$ – $10^{10} \text{ M}^{-1} \text{ s}^{-1}$ —too fast to be measured by stopped-flow techniques.

These electrochemical techniques thus provide a unique tool for estimating rate constants for these reactions at low acid concentrations. These large constants also explain the previously reported striking retardation effect of this complex in the ferric ion catalyzed decomposition of hydrogen peroxide.<sup>21</sup> In this reaction,  $\text{HO}_2\cdot$  radicals oxidize the ferrous to the ferric complex, which undergoes intramolecular reduction faster than it can oxidize  $\text{H}_2\text{O}_2$ , thus causing the regeneration of hydrogen peroxide.

Examples of other ligand-oxidation reactions involving macrocyclic ligands through this general mechanism have been reported.<sup>22–24</sup> In some cases the intermediates with the metal ion in the higher oxidation states have been isolated.<sup>25,26</sup> We propose the use of electrochemical techniques to determine intramolecular reduction rate constants, especially for those cases in which the spectral properties of the species involved do not allow the use of fast photometric or EPR techniques.

**Acknowledgment.** This work was supported in part by the Air Force Office of Scientific Research. H.L.C. acknowledges financial support from the Fundacao de Amparo a Pesquisa do Estado de São Paulo. Valuable discussions with Professor A. J. Bard and Dr. J. H. Christie are gratefully acknowledged.

**Registry No.**  $\text{Fe}(\text{GMI})_3^{2+}$ , 20498-13-9;  $\text{Fe}(\text{GMI})_2(\text{GA})^{3+}$ , 49564-89-8;  $\text{Fe}(\text{GMI})_2(\text{GH})^{2+}$ , 43211-74-1.

## References and Notes

- (1) (a) Universidade de São Paulo. (b) Colorado State University.
- (2) H. L. Chum and P. Krumholz, *Inorg. Chem.*, **13**, 514 (1974).
- (3) H. L. Chum and P. Krumholz, *Inorg. Chem.*, **13**, 519 (1974).
- (4) P. Krumholz, H. L. Chum, M. A. De Paoli, and T. Rabokai, *J. Electroanal. Chem. Interfacial Electrochem.*, **51**, 465 (1974).
- (5) R. S. Nicholson and I. Shain, *Anal. Chem.*, **36**, 706 (1964).
- (6) G. E. B. Randles, *Trans. Faraday Soc.*, **44**, 327 (1948); A. Sevcik, *Collect. Czech. Chem. Commun.*, **13**, 349 (1948).
- (7) A. C. Riddiford, *Adv. Electrochem. Electrochem. Eng.*, **4**, 249 (1967).
- (8) L. S. Marcoux, R. N. Adams, and S. Feldberg, *J. Phys. Chem.*, **73**, 2611 (1969).
- (9) P. A. Malachuk, L. S. Marcoux, and R. N. Adams, *J. Phys. Chem.*, **70**, 4068 (1966).
- (10) L. Marcoux, *J. Am. Chem. Soc.*, **93**, 537 (1971).
- (11) D. Bartak and R. A. Osteryoung, *J. Electroanal. Chem. Interfacial Electrochem.*, **74**, 69 (1976).
- (12) R. N. Adams, "Electrochemistry at Solid Electrodes", Marcel Dekker, New York, N.Y., 1969.
- (13) K. Sone, *Bull. Chem. Soc. Jpn.*, **25**, 1 (1952).
- (14) P. Krumholz, *Struct. Bonding (Berlin)*, **9**, 139 (1971).
- (15) H. Taube, "Electron Transfer Reactions of Complex Ions in Solution", Academic Press, New York, N.Y., 1970, Chapter 4.
- (16) J. H. Christie, private communication.
- (17) S. Richter, C. Daul, and A. V. Zelewsky, *Inorg. Chem.*, **15**, 943 (1976).
- (18) S. Karp, *J. Phys. Chem.*, **72**, 1082 (1968).
- (19) From the cyclic voltammetric data it is possible to make crude estimates of the rate constant as  $(3\text{--}5) \times 10 \text{ s}^{-1}$ . However, due to high double-layer effects at the high scan rates employed, a treatment of the cyclic voltammetric data analogous to that applied to the rotating-disk studies is precluded.
- (20) T. Ruff and M. Zimonyi, *Electrochim. Acta*, **18**, 515 (1973).
- (21) M. L. de Castro and H. L. Chum, *J. Am. Chem. Soc.*, **96**, 5378 (1974).
- (22) V. L. Goedken and D. H. Busch, *J. Am. Chem. Soc.*, **94**, 7355 (1972).
- (23) G. C. Christoph and V. L. Goedken, *J. Am. Chem. Soc.*, **95**, 3869 (1973).
- (24) O. C. Olson and J. Vasilevskis, *Inorg. Chem.*, **10**, 463 (1971).
- (25) N. F. Curtis and D. F. Cook, *Chem. Commun.*, 962 (1967).
- (26) V. L. Goedken, *J. Chem. Soc., Chem. Commun.*, 207 (1972).